Electron scattering from pyrazine: Elastic differential and integral cross sections

P. Palihawadana,[1] J. P. Sullivan,[1] S. J. Buckman,[1,2] and M. J. Brunger[2,3,a)]
[1]*Centre for Antimatter-Matter Studies, Research School of Physics and Engineering, Australian National University, Canberra ACT 0200, Australia*
[2]*Institute of Mathematical Sciences, University of Malaya, 50603 Kuala Lumpur, Malaysia*
[3]*Centre for Antimatter-Matter Studies, CaPS, Flinders University, GPO Box 2100, Adelaide SA 5001, Australia*

(Received 19 October 2012; accepted 1 November 2012; published online 27 November 2012)

We report on new measurements for elastic electron scattering from pyrazine. Absolute differential cross sections (DCSs) at seven discrete energies in the range 3–50 eV, and over the scattered electron angular range 10°–129°, were determined using a crossed electron-molecular beam spectrometer in conjunction with the well-established relative flow technique. Integral elastic cross sections were subsequently derived from those DCS data at each energy. Where possible comparison between the present results and those from sophisticated Schwinger multichannel and R-matrix computations is made, with generally quite good quantitative accord being found. Finally, in order to better study some of the rich resonance structure predicted by theory, results from elastic electron excitation functions are presented. © *2012 American Institute of Physics*. [http://dx.doi.org/10.1063/1.4767570]

I. INTRODUCTION

There have been two relatively recent and quite detailed theoretical investigations into low-energy electron scattering from pyrazine. The first was a Schwinger multichannel computation (SMC) from Winstead and McKoy,[1] conducted at both the static exchange (SE) and incorporating polarisation (SEP) levels, that reported cross sections and investigated the three low-lying π^* shape resonances originally observed in the pioneering, but relative, transmission measurements of Nenner and Schulz.[2] The second was a R-matrix computation,[3] at both the SEP and close coupling (CC) levels and with diffuse and compact basis states to describe the pyrazine target, that also reported elastic, and additionally inelastic, cross sections as well as a detailed analysis of those low-energy shape resonances. In both these studies, a major rationale for their being undertaken was that pyrazine is a good model for the pyrimidinic nucleobases,[1,3] so that it represents an excellent candidate species for employing charged-particle track simulation approaches[4–6] for investigating radiation damage in matter.[7] That rationale also forms part of the basis for us conducting the current study. However, the major rationale for our investigation is that neither Winstead and McKoy[1] nor Mašín and Gorfinkiel[3] could compare the results of their computations against any measured absolute cross section data. Such a comparison potentially provides a detailed validation for their approaches, and is therefore important, so that it provided a major impetus for us to conduct the present measurements. We therefore report absolute elastic differential cross sections (DCSs) for low energy (3–50 eV) electron scattering from pyrazine, with integral cross sections (ICSs), as derived from those DCSs, also being determined.

Pyrazine and pyrimidine are structural isomers, and both can be thought of as being benzene derivatives (see Fig. 1). In addition, all three molecules, to one degree or another, exhibit quite similar physico-chemical properties. For instance, benzene has an isotropic dipole polarisability (α) of ∼68.9 a.u.,[8] with the corresponding value for pyrimidine being ∼59.3 a.u.[9] and that for pyrazine being ∼60 a.u.[10] Similarly, as a consequence of their very high symmetry (see Fig. 1), benzene and pyrazine have no permanent dipole moment, while pyrimidine, on the other hand, has a dipole moment of ∼2.33 D.[11] It is thus interesting, and possibly instructive, to compare the scattering cross sections for these three molecules to see if any trends emerge and whether or not those trends can be associated with their intrinsic physico-chemical properties. Such a comparison is only now possible due to some recent detailed studies on pyrimidine,[12–15] earlier work on benzene[16,17] and the current measurements with pyrazine. Note that this systematic comparison of the scattering behaviour for benzene, pyrimidine, and pyrazine also forms a rationale behind the present work.

Details of the experimental apparatus and techniques are explained in Sec. II, with our results and a discussion of those results, including a detailed comparison with the available theories,[1,3] being given in Sec. III. Finally, in Sec. IV, some concluding remarks are made.

II. EXPERIMENTAL APPARATUS AND TECHNIQUES

A crossed electron-molecular beam apparatus was employed to measure the elastic electron scattering cross sections from pyrazine. A detailed description of this spectrometer has been given previously (e.g., Ref. 18), so that only a précis is given below. Note, however, that since the description in Gibson *et al.*[18] a fully computer-controlled hardware and controlling software to support it have been implemented.

a)Electronic mail: Michael.Brunger@flinders.edu.au.

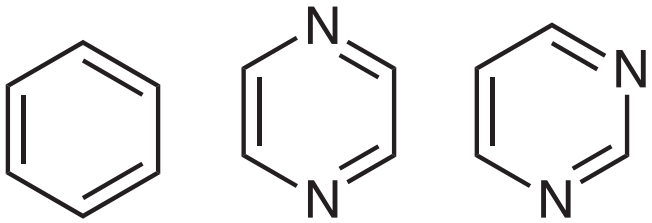

FIG. 1. Schematic diagram showing the structures of benzene, pyrazine, and pyrimidine.

That development assisted with both the optimisation of the incident electron beam current and its energy resolution. In addition, the data acquisition, analysis and real-time monitoring of all the experimental parameters is handled by the new computer system.

In the present study, the spectrometer is operated in two different data collection modes, in order to measure the elastic DCS and the elastic excitation functions (EEFs) for electron scattering from pyrazine. For the DCS measurements, the energy of the incident electron beam is fixed, and the scattered electron analyser is rotated about the molecular beam axis in order to measure the elastic intensity at fixed angles. For the EEF measurements, the analyser is fixed at a given angle, while the energy of the incident beam is ramped over the desired range and the elastic scattering intensity is simultaneously recorded.

The energy of the incident electron beam is calibrated against the position of the well-known $1s2s^2\ ^2S$ negative-ion resonance in the helium (He) elastic channel, at 19.365 eV.[19] The overall energy resolution of the spectrometer is about 70–90 meV (FWHM) for the present experimental results, which implies that our elastic measurements are in fact rotationally averaged. Furthermore, as the lowest vibrational modes of pyrazine can be excited at ~50 meV some vibrational averaging occurs. Depending on the specific energy of the electron beam, the incident beam current, as measured with a Faraday Cup, varied between 0.5–4 nA. The electron beam profile and current were optimised under computer control in order to obtain the best possible signal to background ratio for the scattering experiments. The electron analyser is capable of measuring DCSs and EEFs over an angular range of $\sim -20^\circ$ to 130° about the incident electron beam direction. The angular resolution of the present measurements is typically $\pm 1^\circ$. The true zero position of the analyser is determined by extrapolating to the maximum of the scattered electron signal from measurements on either side of the mechanical zero positions. We estimate this to be accurate to $\pm 0.5^\circ$.

A high-purity (99% or better) colourless crystalline sample of pyrazine, purchased from Sigma-Aldrich, is used to generate the pyrazine vapour. At room temperature the vapour pressure above this sample was typically in the range 8–9 Torr, which was sufficient to provide a stable source for the target molecular beam. The molecular beam is formed by quasi-effusive flow of the gas through a capillary needle, 15 mm long and 0.75 mm in diameter. In this investigation, the temperature of the gas lines and valves that controlled the flow of the gas was kept at around 35 °C – 40 °C, while the capillary temperature was elevated slightly to 40 °C – 45 °C. This helps to prevent any condensation of pyrazine onto the inner walls of the gas lines and valves. Both the pressure and the temperature were monitored and controlled by the new computer-controlled hardware system. The temperature variations during our measurements were within ±1 °C, while the change in the pyrazine pressure was less than 5%.

The relative flow technique[20] is employed to obtain absolute elastic cross sections by comparing the scattered electron signals from pyrazine with those from helium. Helium is used as the reference gas as its elastic DCS are now well established and have been considered as a "benchmark" for many years in this field. For energies below 20 eV, the He cross sections from the variational calculations of Nesbet[21] are used, whereas for higher energies the rational function fits of Boesten and Tanaka[22] to a range of previous measurements (e.g., Ref. 23) of the He cross sections are used. The elastic DCS of pyrazine (Pyr), at a given incident electron energy (E_0) and scattered electron angle (θ), is derived using the formula

$$\mathrm{DCS_{Pyr}}(E_0,\theta) = \frac{N_{\mathrm{Pyr}} - N_{\mathrm{B}}}{N_{\mathrm{He}} - N_{\mathrm{B}}}.\frac{F_{\mathrm{He}}}{F_{\mathrm{Pyr}}}.\sqrt{\frac{M_{\mathrm{He}}}{M_{\mathrm{Pyr}}}}.\mathrm{DCS_{He}}(E_0,\theta), \quad (1)$$

where $\mathrm{DCS_{Pyr}}(E_0,\theta)$ and $\mathrm{DCS_{He}}(E_0,\theta)$ are the absolute DCSs for elastic scattering from pyrazine and He, N_{Pyr} and N_{He} are the measured scattering signals from the pyrazine and helium gases [with the background scattering (N_{B}) contribution subtracted from both measurements], F_{Pyr} and F_{He} are the measured relative flow rates and M_{Pyr} and M_{He} are the molecular weights of Pyr and He, respectively. Note that all the scattering signals (N_{Pyr}, N_{He}, N_{B}) mentioned above are corrected for any variation in the electron beam current during the measurement cycle.

The ratio of the driving pressures between pyrazine and helium is selected to satisfy the condition that the collisional mean free paths are the same in the beam-forming capillary. This is done to ensure that the collision-dependent spatial profile of the gas beams is largely identical in the interaction region. For the present study, this implied a helium to pyrazine ratio ~7.3, with the typical driving pressures for each species being in the range 1–1.2 Torr for helium and 0.135–0.165 Torr for pyrazine. Note that during the course of our measurements we allowed on occasion the helium to pyrazine ratio to vary by up to 15% from the optimum value, with no noticeable effect, to within our measurement uncertainties, being found on the derived pyrazine absolute DCSs. The overall uncertainty, both statistical and systematic, of this work is between 7.3% and 30%, but for the overwhelming majority of determinations it lies below 12%.

III. RESULTS AND DISCUSSION

Our measured absolute DCSs for elastic scattering of electrons from pyrazine are listed in Table I, along with their associated errors (expressed as a percentage of each of the DCSs). Also included in Table I at the foot of each column are the absolute ICS (and precentage error) for each incident energy. In Figs. 2(a)–2(g), we compare the present DCS

TABLE I. Absolute experimental DCSs for elastic scattering from pyrazine in units of 10^{-16} cm^2 sr^{-1}. The uncertainty is given in parentheses (%). The ICS for each incident energy is given in units of 10^{-16} cm^2 at the base of each column. The uncertainty on the ICS is also given in parentheses (%).

Scattering angle (°)	Incident energy (eV)						
	3	6	10	15	20	30	50
10							44.6 (7.6)
20				19.2 (24)	12.3 (7.9)	10.4 (8.7)	5.58 (7.3)
30	3.18 (24)	7.87 (30)	8.10 (15)	6.92 (8.6)	3.13 (7.5)	2.51 (9.8)	1.28 (7.9)
40	3.32 (7.7)	6.14 (23)	5.78 (12)	1.63 (8.7)	0.977 (8.7)	0.960 (10)	0.979 (7.4)
50	3.35 (7.4)	4.22 (17)	2.87 (8.2)	0.847 (7.4)	0.676 (8.1)	1.01 (11)	0.716 (8.3)
60	3.20 (8.1)	2.91 (16)	1.55 (7.9)	0.967 (7.7)	0.859 (7.7)	0.671 (10)	0.364 (7.6)
70	2.71 (7.4)	1.93 (12)	1.32 (7.8)	1.09 (7.3)	0.798 (7.5)	0.458 (11)	0.269 (8.7)
80	1.90 (7.6)	1.19 (8.6)	1.47 (7.5)	1.03 (7.3)	0.695 (7.5)	0.387 (11)	0.244 (7.8)
90	1.35 (9.1)	1.09 (8.8)	1.44 (7.7)	0.969 (7.3)	0.689 (7.3)	0.371 (10)	0.244 (7.7)
100	0.942 (17)	1.25 (8.6)	1.62 (7.9)	0.891 (7.5)	0.703 (7.4)	0.407 (8.9)	0.255 (7.8)
110	0.870 (7.6)	1.80 (7.4)	1.58 (7.6)	0.889 (11)	0.808 (7.9)	0.486 (9.0)	0.314 (7.6)
120	0.953 (9.4)	2.03 (8.0)	1.48 (7.7)	1.08 (7.5)	0.945 (7.4)	0.672 (8.3)	0.384 (8.0)
129	1.11 (11)	2.43 (9.1)	1.56 (8.0)	1.20 (6.8)	0.961 (8.3)	0.812 (12)	0.471 (7.8)
ICS	34.7 (25)	36.5 (32)	48.0 (25)	34.9 (25)	35.6 (20)	23.7 (20)	16.5 (20)

measurements at 3, 6, 10, 15, 20, 30, and 50 eV, respectively, with earlier SMC[1] and R-matrix[3] results (where possible). There are no previous DCS pyrazine measurements that we are aware of, however, corresponding results for scattering from benzene[16,17] and pyrimidine[12] are included throughout the plots that comprise Fig. 2. Our measured ICSs are shown in Fig. 3, where they are compared against the available theory.[2,3] Finally, in Fig. 4 we present the current EEF measurements, at scattering angles of (a) 60°, (b) 90°, and (c) 120° for the 3–15 eV energy range, along with the corresponding DCS measurements.

Considering now Fig. 2(a) for an impact energy of 3 eV in more detail, we observe very good quantitative agreement between the present measurements and both the SMC-SEP[1] and R-matrix-SEP with a diffuse basis set[3] calculations, to within the uncertainties on our measurements. On the other hand, none of the other three R-matrix computations, i.e., SEP-compact basis and CC diffuse and compact basis states, predict the shape of the 3 eV angular distribution below about $\theta = 60°$. This observation is consistent with the expectation of Mašín and Gorfinkiel,[3] who anticipated that below the third π^* resonance in pyrazine[2] (at about 4 – 4.1 eV) their R-matrix-SEP, with a diffuse basis to describe the target, would be the most physical calculation. Note, however, that above 4.1 eV this R-matrix calculation is soon affected by the presence of many pseudoresonances (see Fig. 3), so that above this energy their preferred result, i.e., the most physical result, is the R-matrix-CC plus compact basis calculation.[24] The shape of the 3 eV elastic pyrazine angular distribution is very interesting, with the cross section "flattening out" and perhaps even "turning over" in value at scattering angles less than 60°. This is contrary to the behaviour for all the other measured angular distributions, at energies from 6–50 eV [see Figs. 2(b)–2(g)], which have cross sections that are forward peaked in magnitude as you go to smaller θ, with this degree of forward peaking in the angular distribution increasing as the incident electron energy increases. This interesting behaviour in the 3 eV elastic angular distribution is, however, not unique. We have also observed it previously, typically in the energy range ~1.5–8.5 eV, the actual range depending on the species under investigation, in such diverse molecules as O_2,[25,26] NO,[27] CO_2,[28] benzene[16] and pyrimidine[12] (to name just a few). One rationale, that has previously been advanced,[29] explains the observed behaviour in terms of the dynamical polarisation of the targets in question. In any event, a definitive explanation for this phenomenon still awaits detailed computational studies from our theoretical colleagues.

The expectation of Mašín and Gorfinkiel[3,24] that above ~4.1 eV their R-matrix calculation, using a close coupling approach with a compact basis set description, would provide their most physical description for the elastic scattering process appears borne out by Figs. 2(b)–2(d), at 6 eV, 10 eV, and 15 eV, respectively. At each of those energies that computation is seen to be in quite good, although not perfect, quantitative agreement with the present measurements and certainly is in better accord with the data than either of the R-matrix–SEP level or the R-matrix–CC–diffuse level results. This is perhaps a little surprising at 10 eV and 15 eV, as R-matrix computations above the ionisation threshold of a target (for pyrazine the ionisation threshold = 9.4 eV[30]), where they do not incorporate pseudostates such as in this case, should be treated with a little caution.[24] Nonetheless the evidence here in Figs. 2(c) and 2(d) clearly suggests this approach is providing a satisfactory description in this case. Particularly at 6 eV (Fig. 2(b)), the SMC–SEP calculation also does a very good job in reproducing the measured data, in terms of both the shape and magnitude of the cross section. At 10 eV [Fig. 2(c)] and 15 eV [Fig. 2(d)], however, while it still provides a quantitative description of the DCS for $\theta < 40°$, at higher angles the SMC–SEP result begins to somewhat systematically overestimate the magnitude of the cross sections although the shape accord remains very good.

In Figs. 2(e)–2(g), we show the present higher energy 20 eV, 30 eV, and 50 eV DCSs, respectively, and again compare them to the available theoretical results. For the DCS at 20 eV [Fig. 2(e)], this entails a comparison with the SMC

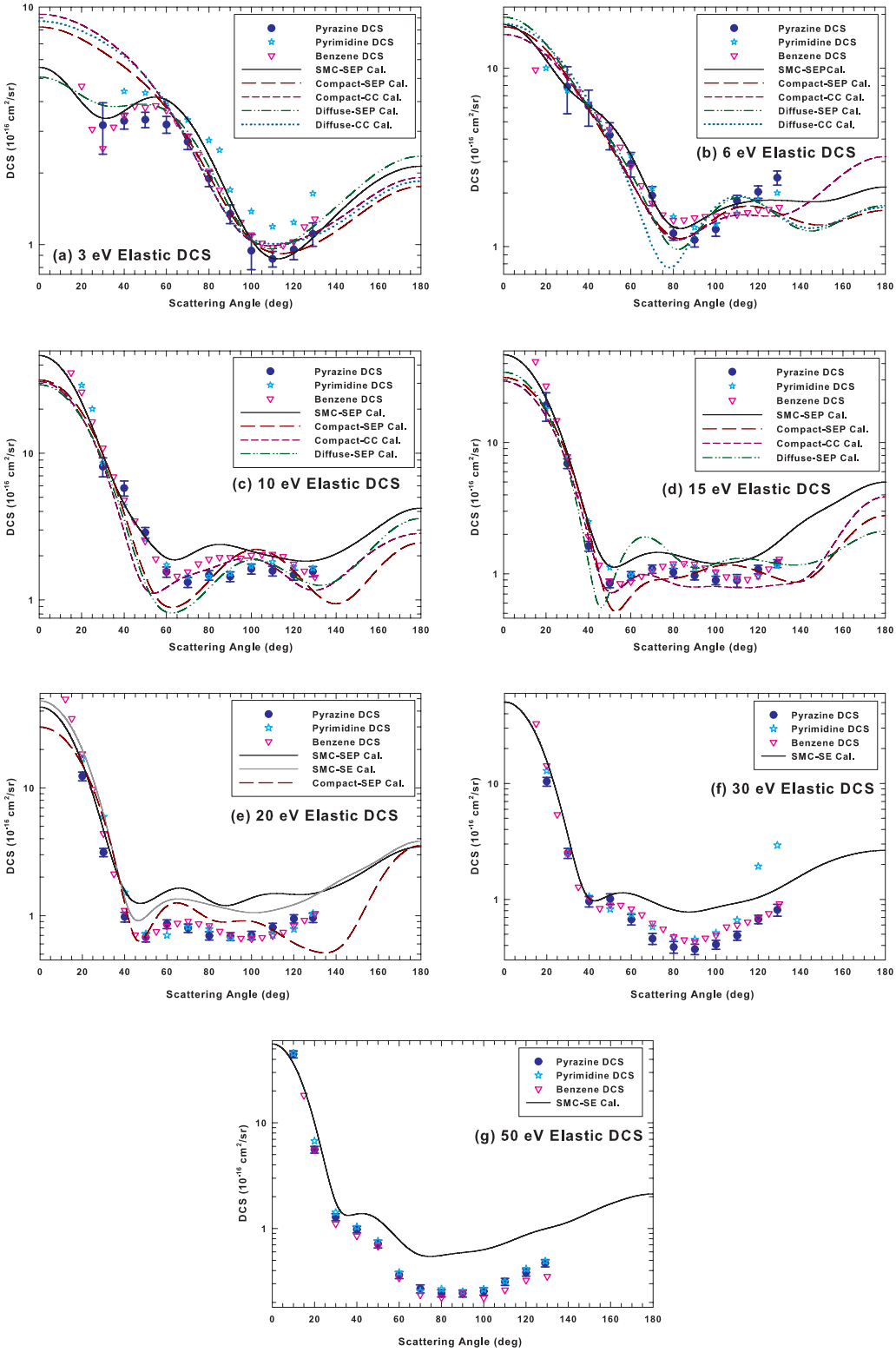

FIG. 2. Absolute DCS (10^{-16} cm^2 sr^{-1}) for elastic electron scattering from pyrazine at (a) 3 eV, (b) 6 eV, (c) 10 eV, (d) 15 eV, (e) 20 eV, (f) 30 eV, and (g) 50 eV. The present pyrazine measurements are shown as full circles, with earlier benzene results[16,17] denoted by inverted triangles and pyrimidine data[12] by stars. The SMC theory results[1] are shown as solid curves, while the various R-matrix calculations at the SEP and CC levels, for compact and diffuse basis sets are, respectively, represented by long dashed curves, short dashed curves, dotted curves, and dashed-dotted curves. See also the legend on each pane.

results at both the static exchange and static exchange plus polarisation levels, while for the R-matrix approach we are now limited to a calculation at the SEP with compact basis level. Both the SMC–SEP and R-matrix–SEP computations suggest structure in the angular distribution which is not observed experimentally. This perhaps indicates that there are some convergence issues with those theoretical results at this energy. Nonetheless the R-matrix–SEP calculation appears to still be providing a reasonable description for the scattering dynamics at 20 eV, particularly when one allows for the fact that

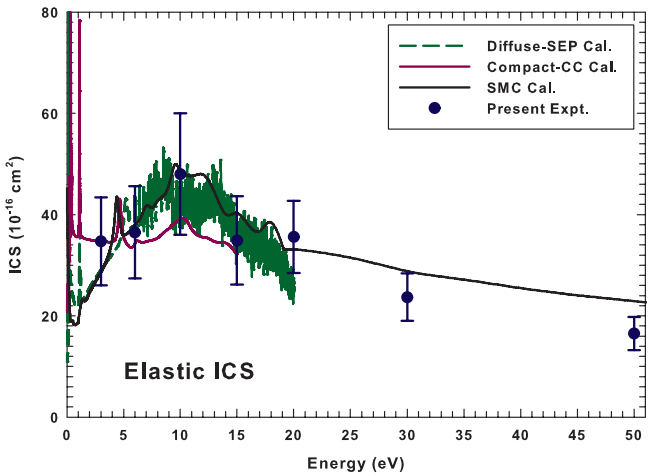

FIG. 3. Present ICSs (10^{-16} cm^2) for elastic electron scattering from pyrazine. The present pyrazine measurements are shown as full circles, while the SMC theory result[1] is depicted as a solid black curve. The R-matrix result at the SEP level and with a diffuse basis[3] is denoted by a dashed green curve, while the close-coupling R-matrix computation with a compact basis[3] is represented by the solid purple curve. See also the legend on the figure.

we are now well above the ionisation threshold of pyrazine. Perhaps the best shape agreement at 20 eV is between the present data and the SMC–SE result, although the SMC-SE calculation, roughly for $\theta > 40^\circ$, does systematically overestimate the magnitude for this cross section. For 30 eV [Fig. 2(f)] and 50 eV [Fig. 2(g)] we are now only able to compare our DCSs against the SMC–SE results, with the story found basically being the same in each case. Namely, while the calculation does a very good job in reproducing the shapes of the angular distribution at both energies it fails, for $\theta > 30^\circ - 50^\circ$ depending on the energy, to predict its magnitude at the middle and backward angles. This is not a surprising result, with exactly the same behaviour being found in our previous joint theory/experimental study with pyrimidine[12] at these higher energies. Recently, for a number of quite complicated targets,[31–33] the independent atom model with screening corrected additivity rule (IAM–SCAR) theoretical approach has been demonstrated to provide good quantitative agreement with measured data for incident electron energies above about 20 eV. It would, therefore, be very interesting if the Spanish group[31–33] were also to apply their approach to pyrazine.

Throughout Figs. 2(a)–2(g), we have also plotted corresponding results from our earlier studies of elastic electron scattering from pyrimidine[12] and benzene.[16,17] With the exception of 3 eV, the level of agreement between the measured DCS for pyrazine, benzene, and pyrimidine, in each of Figs. 2(b)–2(g), is really remarkably good. Where minor disagreements, outside of the errors in all three measurements, do exist they may simply reflect the small differences in the dipole polarisabilities of the three species. Recall (see the Introduction) that $\alpha \sim 68.9$ a.u. for benzene, $\alpha \sim 59.3$ a.u. for pyrimidine, and $\alpha \sim 60$ a.u. for pyrazine. Also remember that while $\mu = 0$ D for benzene and pyrazine, $\mu \sim 2.33$ D for pyrimidine (again see the Introduction). Hence the level of agreement we see between the DCSs for these 3 species, in Figs. 2(b)–2(g), might indicate the very important role played

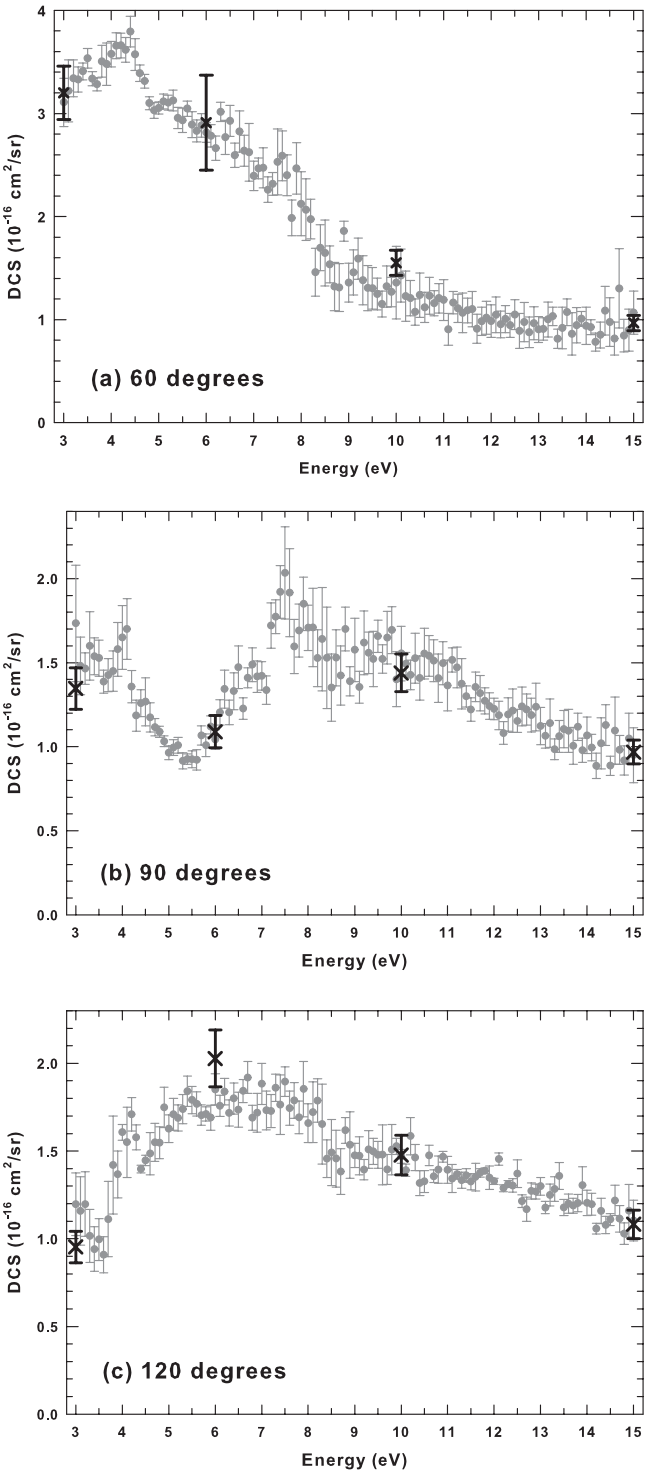

FIG. 4. Absolute DCSs (10^{-16} cm^2 sr^{-1}) shown as a function of energy (EEF) for the energy range 3–15 eV (•), at the scattering angles of (a) 60°, (b) 90°, and (c) 120°. Also shown are the angular DCS measurements (×) taken at discrete energies in the range of interest.

by the dipole polarisability in the scattering dynamics of each of these molecules, with their similar values for α reflecting the similar DCSs we measure. This same behaviour is also found for benzene and pyrazine in Fig. 2(a) at 3 eV, although now the magnitude of the DCSs for pyrimidine appear to be somewhat systematically larger in value than those for benzene and pyrazine. In this case, we believe the observed

results are indicative for an enhanced rotational contribution to the pyrimidine elastic signal (recall we can never discriminate against such a contribution with our typically achieved energy resolution), as brought about by the permanent dipole moment of pyrimidine. Notwithstanding our preceding discussion on the role of the dipole polarisability in the behaviour observed in Figs. 2(b)–2(g), we should note that all three species also possess other similar physico-chemical properties (e.g., shape, size, and valence electronic structure) which may play equally important roles in terms of the scattering dynamics of those systems.

From the above discussion, we can conclude that there is a good shape agreement between the present measured DCS and the SMC–SEP calculation for energies between 3–15 eV, and between the present DCS and SMC–SE calculation for energies between 20–50 eV. As a consequence, at each energy, we have employed the shape of the relevant SMC computation to extrapolate our measured data to 0° and 180°. That data are then integrated and multiplied by 2π, resulting in an experimental estimate of the elastic ICS at each energy. Those ICS can be found at the foot of Table I and are plotted in Fig. 3, along with the corresponding SMC results and the R-matrix results at the SEP-level with a diffuse basis set to describe the target and at the CC-level with a compact target representation. Note that due to the additional uncertainty caused by our extrapolation, we conservatively estimate the errors on our ICS to be in the 20%–32% range. Having said that, however, pyrazine is a non-polar molecule so that the forward angle extrapolation we employed, using the SMC results, should be quite sound in this case. It is apparent from Fig. 3 that for energies less than and equal to 20 eV, the present ICS, to within our stated uncertainties, are in fair accord with both the SMC–SEP and R-matrix results. The problem the R-matrix–SEP calculation has with pseudoresonances, above the third π^* resonance[2] at around 4 eV, is also clear from this figure. For energies above 20 eV, we see in Fig. 3 that the only available SMC–SE theory overestimates the magnitude of the elastic ICS at both 30 eV and 50 eV. This result is consistent with our expectation, based on the comparison between the experimental and theoretical DCS at 30 eV and 50 eV. It would be interesting to see how the present higher energy ($E_0 \geq 20$ eV) integral cross sections compared to results calculated from an IAM–SCAR approach for pyrazine. Based on what we found in pyrimidine,[12] we anticipate that the agreement might be rather good.

One of the problems with deriving ICSs at discrete energies, such as we have done here, is also apparent from Fig. 3. Namely, that potentially rich resonance structure (as predicted by theory) is likely to be missed. To circumvent this limitation, we have therefore also measured elastic excitation functions at three scattered electron angles, $\theta = 60°$, 90°, and 120°, with the results from those measurements in the 3–15 eV energy range being shown in Fig. 4. It is apparent from Fig. 4 that the elastic data we measured in the excitation function mode are entirely consistent with those acquired through our angular distribution measurements. This is true at each of 60°, 90°, and 120° and, therefore, gives us some confidence in the validity of our experiments. The third low-energy π^* resonance in pyrazine[1–3] is clearly visible in our elastic excitation functions, suggesting a peak energy in the region ~4.1–4.3 eV. This result compares favourably with the experimental value from the transmission measurement of Nenner and Schulz[2] at ~4.1 eV, and with the SMC result[1] at 4.4 eV and the preferred R-matrix close coupling value at 4.58 eV.[3] That the theoretical resonance energies from both calculations[1,3] are a little higher than the corresponding measured values was anticipated by both Winstead and McKoy[1] and Mašín and Gorfinkiel[3] and reflects some limitations in their respective approaches. Nonetheless, we would characterise this overall level of accord between experiment and theory, for the position of this shape resonance, as being rather good.

IV. CONCLUSIONS

We have reported original measurements for differential and integral cross sections for elastic electron scattering from pyrazine. Agreement, for energies less than about 20 eV, with available R-matrix and SMC–SEP level calculations was typically found to be good. At the higher energies, however, while good shape accord was found between our measurements and the only available SMC–SE results, the theory overestimated the magnitude of the differential cross sections at middle and backward angles. These observations at the DCS level were, as expected, also reflected between theory and experiment for the integral cross sections. A comparison of the present elastic pyrazine DCS results, with previous DCSs for pyrimidine and benzene, showed a remarkable level of agreement between them to within the various experimental uncertainties. This accord seemed in some way to correlate with the similar structures and dipole polarisabilities of the three species. Only at 3 eV was there clear evidence for the effect of the permanent dipole moment of pyrimidine, compared to non-polar pyrazine and benzene, on the scattering dynamics. Finally, we noted that it would be very interesting to compare, at $E_0 \geq 20$ eV, results from IAM–SCAR calculations to the present data. Elastic excitation function data measured as a part of this study determined the third low-energy π^* resonance peak to occur in the range ~4.1–4.3 eV, in pretty good agreement with that from an earlier transmission measurement and with results from available SMC and R-matrix calculations.

ACKNOWLEDGMENTS

Partial financial support from the Australian Research Council through its Centres of Excellence program is acknowledged. We thank Carl Winstead, Zdeněk Mašín, and Jimena Gorfinkiel for providing us with tabulated data for their calculated results. We further thank Dr. M. V. Perkins for supplying us with Fig. 1, and Dr. L. Campbell for his assistance in some aspects of the production of this paper. Finally, one of us (P.P.) thanks the Australian National University for his postgraduate scholarship.

[1] C. Winstead and V. McKoy, Phys. Rev. A **76**, 012712 (2007).
[2] I. Nenner and G. J. Schulz, J. Chem. Phys. **62**, 1747 (1975).
[3] Z. Mašín and J. D. Gorfinkiel, J. Chem. Phys. **135**, 144308 (2011).

[4]A. Muñoz, F. Blanco, G. García, P. A. Thorn, M. J. Brunger, J. P. Sullivan, and S. J. Buckman, Int. J. Mass Spectrom. **277**, 175 (2008).
[5]I. Plante and F. A. Cucinotta, New J. Phys. **11**, 063047 (2009).
[6]A. G. Sanz, M. C. Fuss, A. Muñoz, F. Blanco, P. Limão-Vieira, M. J. Brunger, S. J. Buckman, and G. García, Int. J. Radiat. Biol. **88**, 71 (2012).
[7]B. D. Michael and P. O. Neil, Science **287**, 1603 (2000).
[8]A. Hinchliffe and H. J. S. Machado, Int. J. Mol. Sci. **1**, 8 (2000).
[9]A. Zecca, L. Chiari, G. Garcia, F. Blanco, E. Trainotti, and M. J. Brunger, J. Phys. B **43**, 215204 (2010).
[10]See http://cccbdb.nist.gov/ for relevant physico-chemical data.
[11]G. L. Blackman, R. D. Brown, and F. R. Burden, J. Mol. Spectrosc. **35**, 444 (1970).
[12]P. Palihawadana, J. Sullivan, M. Brunger, C. Winstead, V. McKoy, G. Garcia, F. Blanco, and S. Buckman, Phys. Rev. A **84**, 062702 (2011).
[13]D. B. Jones, S. M. Bellm, F. Blanco, M. Fuss, G. García, P. Limão-Vieira, and M. J. Brunger, J. Chem. Phys. **137**, 074304 (2012).
[14]Z. Mašín, J. D. Gorfinkiel, D. B. Jones, S. M. Bellm, and M. J. Brunger, J. Chem. Phys. **136**, 144310 (2012).
[15]D. B. Jones, S. M. Bellm, P. Limão-Vieira, and M. J. Brunger, Chem. Phys. Lett. **535**, 30 (2012).
[16]H. Cho, R. J. Gulley, K. Sunohara, K. Kitajima, L. J. Uhlmann, H. Tanaka, and S. J. Buckman, J. Phys. B **34**, 1019 (2001).
[17]H. Kato, M. C. Garcia, T. Asahina, M. Hoshino, C. Makochekanwa, H. Tanaka, F. Blanco, and G. García, Phys. Rev. A **79**, 062703 (2009).
[18]J. C. Gibson, L. A. Morgan, R. J. Gulley, M. J. Brunger, C. T. Bundschu, and S. J. Buckman, J. Phys. B **29**, 3197 (1996).
[19]A. Gopalan, J. Bömmels, S. Götte, A. Landwehr, K. Franz, M.-W. Ruf, H. Hotop, and K. Bartschat, Eur. Phys. J. D **22**, 17 (2003).
[20]M. J. Brunger and S. J. Buckman, Phys. Rep. **357**, 215 (2002).
[21]R. K. Nesbet, Phys. Rev. A **20**, 58 (1979).
[22]L. Boesten and H. Tanaka, At. Data Nucl. Data Tables **52**, 25 (1992).
[23]M. J. Brunger, S. J. Buckman, L. J. Allen, I. E. McCarthy, and K. Ratnavelu, J. Phys. B **25**, 1823 (1992).
[24]Z. Mašín and J. D. Gorfinkiel, private communication (2012).
[25]J. P. Sullivan, J. C. Gibson, R. J. Gulley, and S. J. Buckman, J. Phys. B **28**, 4319 (1995).
[26]M. A. Green, P. J. O. Teubner, B. Mojarrabi, and M. J. Brunger, J. Phys. B **30**, 1813 (1997).
[27]B. Mojarrabi, R. J. Gulley, A. G. Middleton, D. C. Carwright, P. J. O. Teubner, S. J. Buckman, and M. J. Brunger, J. Phys. B **28**, 487 (1995).
[28]J. C. Gibson, M. A. Green, K. W. Trantham, S. J. Buckman, P. J. O. Teubner, and M. J. Brunger, J. Phys. B **32**, 213 (1999).
[29]S. J. Buckman, private communication (2012).
[30]D. M. P. Holland, A. W. Potts, L. Karlsson, M. Stener, and P. Decleva, Chem. Phys. **390**, 25 (2011).
[31]H. Kato, K. Anzai, T. Ishihara, M. Hoshino, F. Blanco, G. García, P. Limão-Vieira, M. J. Brunger, S. J. Buckman, and H. Tanaka, J. Phys. B **45**, 095204 (2012).
[32]H. Kato, A. Suga, M. Hoshino, F. Blanco, G. García, P. Limão-Vieira, M. J. Brunger, and H. Tanaka, J. Chem. Phys. **136**, 134313 (2012).
[33]O. Zatsarinny, K. Bartschat, G. Garcia, F. Blanco, L. R. Hargreaves, D. B. Jones, R. Murrie, J. R. Brunton, M. J. Brunger, M. Hoshino, and S. J. Buckman, Phys. Rev. A **83**, 042702 (2011).